Effect of CO_2 laser-induced crystallization on ErF_3-doped tellurite-germanate oxy-fluoride glass

Magdalena Leśniak,[*1] Patryk Zając,[2] Wojciech Talik,[3] Magdalena Ziąbka,[1] Piotr Jeleń,[1] Marcin Kochanowicz,[3] Piotr Miluski,[3] Witold Zawadzki,[2] Krzysztof Dzierżęga,[2] Dominik Dorosz[1]

[1]*Faculty of Materials Science and Ceramics, AGH University of Krakow, Al. Mickiewicza 30, 30-059 Krakow*
[2]*Marian Smoluchowski Institute of Physics, Jagiellonian University, ul. Łojasiewicza 11, 30-348 Krakow*
[3]*Faculty of Electrical Engineering, Bialystok University of Technology, ul. Wiejska 45D, Białystok, 15-351*

Received February 06, 2025; accepted March 25, 2025; published March 31, 2025

Abstract—Glass-ceramic materials, obtained through controlled crystallization of glasses, combine the advantageous properties of both glasses and crystals, making them useful for optical applications. Conventional thermal treatment technique is widely used to induce crystallization in glass. Laser-induced crystallization (LIC) provides a localized and controlled method to modify the glass structure and tailor its optical properties. This study investigates the structural and luminescent properties of Er^{3+}-doped tellurite-germanate glass-ceramic obtained through CO_2 laser irradiation of the parent glass. The observed structural changes induced by laser irradiation led to the crystallization of BaF_2, enhancing the luminescent properties of the material.

Rare-earth (RE)-doped glass-ceramic materials have been extensively studied due to their ability to combine the advantageous optical properties of glasses with the superior luminescent performance of embedded nanocrystals (NCs) [1]. These materials are particularly relevant for applications in optoelectronics, including sensors, amplifiers, and lasers. Among various non-silica glasses based on heavy metal oxides, tellurite-germanate glasses have drawn interest due to their lower phonon energy (~ 850 cm^{-1}), high nonlinear optical properties, and transparency in the range of the visible to mid-infrared (VIS-MIR). These features make them promising candidates for applications in optical amplifiers, lasers, and mid-infrared photonic devices [2]. Further enhancement of the luminescent properties of RE-doped glasses can be achieved by incorporating nanocrystals into the glass matrix, followed by the localization of active ions within nanocrystals characterized by low phonon energy. This effect has been demonstrated for BaF_2 nanocrystals, where their low phonon energy (~240 cm^{-1}) enhances the emission efficiency of rare-earth ions by suppressing non-radiative relaxation processes [3]. Several methods can be employed to achieve crystallization in glass, with the most common being conventional heat-treatment of glass. Another technique involves the direct doping of nanocrystals into the glass matrix, enabling precise control over composition and phase distribution [4].

* E-mail: mlesniak@agh.edu.pl

Contrary to the above methods, laser-induced crystallization (LIC) has emerged as a promising technique, enabling the crystallization of glass by utilizing the localized energy deposition of a laser beam. This process concentrates thermal energy within a confined glass region, promoting nucleation and crystal growth exclusively in the irradiated area while preserving the surrounding amorphous matrix [5]. The CO_2 laser, operating at a wavelength of 10.6 μm, is particularly effective in oxide glasses crystallization, due to its absorption by the glass network [6]. Despite the advantages of CO_2-LIC, such as its capability to induce space-selective nucleation sites, control crystal growth, and enable microstructural patterning in glass-ceramic materials, the underlying crystallization mechanisms in tellurite-germanate glass remain poorly understood [6]. The interaction between CO_2 laser irradiation and the glass matrix, as well as its influence on structural reorganization, phase formation, and luminescence properties of glass-ceramic materials doped with rare-earth ions, requires further investigation. This paper deals with understanding how CO_2 laser-induced crystallization influences the formation and distribution of BaF_2 nanocrystals in tellurite-germanate glass matrix, and their impact on Er^{3+} luminescence is essential for optimizing these materials for photonic applications.

The glass sample in the $30TeO_2$-$23GeO_2$-$10Ga_2O_3$-$20BaF_2$-$10ZnF_2$-$5Na_2O$-$2ErF_3$ (mol%) system was prepared using the melt-quenching method, then cut into 15 mm × 10 mm × 2 mm pieces and polished to achieve an optical quality surface. The glass was irradiated with a CO_2 laser at varying intensities from 4 to 16 W/cm^2 to analyze crystallization tendency. For CO_2 LIC, an intensity of 14.98 W/cm^2 was selected as barium fluoride (BaF_2) crystals formed within the glass matrix, growing to micrometer-scale dimensions. Below this threshold, no crystalline phase formation was observed.

In the experiment of CO_2, the laser-induced crystallization process was performed in dynamic mode under carefully controlled conditions: including laser intensity of 14.98 W/cm^2, a scanning speed of 1 mm/s, and a line length of 5 mm. The glass sample was

preheated on a hot plate at 300°C throughout the laser processing to mitigate thermal stress and prevent cracking due to rapid heating.

The x-ray diffraction (XRD) pattern of the glass-ceramic material (GC) obtained via CO_2 laser-induced crystallization is presented in Fig.1. The diffraction pattern exhibits characteristic peaks at approximately 25°, 29°, 42°, 49°, 61° and 66° (2θ), which correspond to the crystalline phase of barium fluoride (BaF_2) [7]. The XRD pattern also reveals a typical amorphous halo in the 2θ range of 20°–35°, indicating the presence of residual glass.

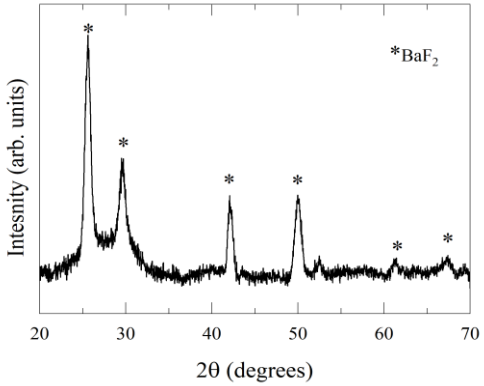

Fig. 1. X-ray diffraction (XRD) pattern of the glass-ceramic material, confirming the presence of crystalline phases.

Figure 2 presents a scanning electron microscopy (SEM) image with point chemical composition analysis (EDS) performed at five different points of the glass-ceramic material, demonstrating a uniform distribution of nanocrystals within the glass matrix. The average crystallite size was estimated to be approximately 40 nm, confirming nanoscale crystallization. The EDS analysis revealed an increased concentration of barium and fluorine in the brighter regions compared to the glass matrix, further confirming the formation of the BaF_2 nanocrystals.

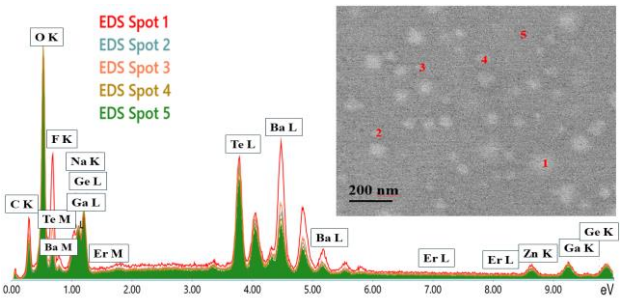

Fig. 2. SEM-EDS images of BaF_2 nanocrystals embedded in the glass matrix.

The near-infrared luminescence spectra of the glass and glass-ceramic material in the 1400–1700 nm spectral range, recorded under an excitation wavelength of λ_{exc} = 976 nm, are presented in Fig. 3.

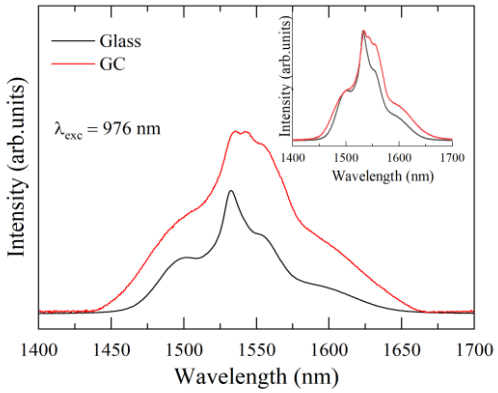

Fig. 3. NIR emission spectra of glass and glass ceramics under 976nm LD excitation. The inset presents comparison of FWHM.

The dominant emission band, centered around 1550 nm, corresponds to the $^4I_{13/2} \rightarrow {}^4I_{15/2}$ electronic transitions in Er^{3+} ions widely used in telecommunication [8]. A comparative spectral analysis revealed the increase in the intensity of the bands as well as full width at half maximum (FWHM) of the emission band from 78 nm in the glass to 97 nm in the glass-ceramic material (Fig. 3 inset). This broadening is related with the change of the local environment of Er^{3+} ions. Moreover, it is probable that induced structural rearrangements were accompanied with the formation of a crystalline BaF_2 phase [9]. Additional evidence of local crystalline environmental (BaF_2) of Er^{3+} ions is a Stark splitting clearly noticeable above 1550 nm wavelength [10].

The Raman spectra, presented in Fig. 4 compare the vibrational characteristics of the glass and glass-ceramic material within the 370–1000 cm^{-1} range. The broad Raman bands for both the glass and glass-ceramic materials comprises multiple overlapping vibrational components. These components were isolated by fitting a sum of Voigt functions. This approach enabled the identification of individual vibrational contributions, providing insight into the structural modifications associated with CO_2 laser-induced crystallization in glass. The fitting of Voigt profiles to the Raman spectra of the glass and glass-ceramic (GC) material reveals five bands centered around 455, 510, 690, 777, and 865 cm^{-1}, which can be assigned to the stretching vibrations of Te-O-Te bridges formed by shared corners of $[TeO_4]_{tbp}$, $[TeO_{3+1}]$, and $[TeO_3]_{tp}$ units [11], symmetric stretching vibrations along the Ge-O-Ge chain [12], antisymmetric stretching vibration of Te-O bond in the $[TeO_4]$ bipyramid [13], stretching of $Te\text{-}O^-$ bonds in $[TeO_3]_{tp}$ and $[TeO_{3+1}]$ units [14], and symmetric stretching of $Ge\text{-}O^-$ bonds in Ge(3) units [15], respectively.

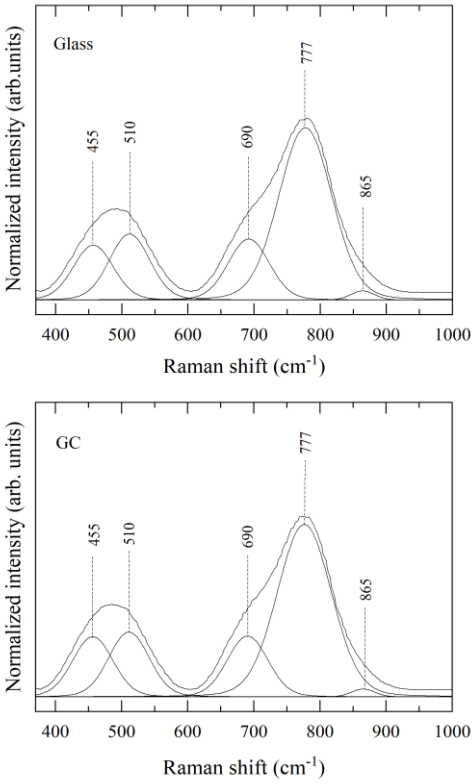

Fig. 4. Fitted Voigt profiles to the Raman spectrum of the glass and glass-ceramic material.

Based on the comparison of the integral intensities (Int.) of the component bands (Table 1), one can observe that the integral intensity of the band at 455 cm^{-1} increased in the glass-ceramic material compared to the glass from 44 to 49 arb. units. This indicates an increase in Te-O-Te bridges in the glass matrix of GC material. Such a reorganization of the glass network facilitates the incorporation of Er^{3+} ions into the structure of BaF_2 nanocrystals, leading to the broadening of the emission band in the 1.5 μm range. As a result, controlled crystallization enhances the luminescent properties of the material, improving emission efficiency (Figure 3).

Table 1. Integral intensities of the component bands in Glass and GC.

Band position (cm^{-1})	455	510	690	777	865
Int. G	44	54	50	185	4
Int. GC	49	53	50	186	3

The results of this study demonstrate that CO_2 laser-induced crystallization (LIC) can be successfully applied to initiate and grow of BaF_2 nanocrystals in the tellurite-germanate glass. Partly, NCs are embedded with Er^{3+} ions, which is confirmed by broaden emission at 1.5 μm. The following issues must be solved to assess the potential of this approach fully and move to application in the development of functional glass-ceramic materials for photonic devices. Understanding the nucleation and growth mechanism of the BaF_2 nanocrystals under CO_2 laser irradiation remains unclear. Analysis of the relationship between processing parameters and crystallization behavior should clarify the role of localized heating, thermal gradients, and structural rearrangements in crystallization. Systematic investigations, including an optimized range of laser power, scanning speeds, and preheating conditions are necessary to control crystal size and distribution. While the shape of the emission band was observed, a more detailed investigation of the relationship between the structural environment of Er^{3+} ions and their optical properties is required. Addressing these directions will be crucial for the understanding and practically applying laser-induced crystallization in rare-earth-doped oxyfluoride glasses.

This work was supported by the National Science Center, Poland [No. 2020/39/D/ST5/02287] and the program Excellence Initiative – Research University for AGH University of Krakow [No. 501.696.7996-L34 (ID: 4844)]. The SEM-EDS investigations were supported by the program Excellence Initiative – Research University for the AGH University of Krakow, grant ID 1449.

References

[1] D.F. Franco, F.J. Caixeta, L.V. Albino, T.A. Lodi, J.R. Orives, E.O. Ghezzi, M. Nalin, Opt. Mater.: X. **20**, 100272 (2023).
[2] Y. Wu, C. Niu, L. Wang, M. Yang, S. Zhang, J. Lumin. **266**, 120323 (2024).
[3] E.E. Brown, Z.D. Fleischman, J. McKay, M. Dubinskii, Opt. Mater. Expr. **11**, 575 (2021).
[4] F.J. Deubener, M. Allix, M.J. Davis, A. Duran, T. Höche, T. Honma, T. Komatsu, S. Krüger, I. Mitra, R. Müller, S. Nakane, M.J. Pascual, J.W.P. Schmelzer, E.D. Zanotto, S. Zhou, J. Non-Cryst Solids. **501**, 3 (2018).
[5] R. Que, M. Lancry, M. Cavillon, B. Poumellec, Crystals **14**, 606 (2024).
[6] F. Mona, N.S. Yazd, A. Keshavarzi, A. Doosti, Cryst. Eng. Comm. **24**, 2753 (2022).
[7] J. Chacaliaza-Ricaldi, V.A.G. Rivera, I.C. Pinto, Y. Messaddeq, E. Marega, J. Non-Cryst. Solids. **638**, 123063 (2024).
[8] Y. Ren, J. Dong, W.Wang, J. Li, X. Cao, Q. Song, M. Wu, X. Qian, Y. Xue, Q. Wang, H. Tang, X. Xu, J. Xu, J. Lumin. **275**, 120743 (2024).
[9] S. Ibrahim, A.A. El-Kheshen, M. Abdel-Baki, A.M. Fayad, Y.M. Hamdy, M.M. Ibrahim, M.A. Marzouk, Ceram. Internal. 51, 458 (2025).
[10] A. Bitam, S. Khiari, M. Diaf, H. Boubekri, E. Boulma, C. Bensalem, L. Guerbous, J.P. Jouart, Opt. Mater. **82**, 104 (2018).
[11] G. Guery, A. Fargues, T. Cardinal, M. Dussauze, F. Adamietz, V. Rodriguez, J.D. Musgraves, K. Richardson, P. Thomas, Chem. Phys. Lett. **554**, 123 (2012).
[12] H.O. Tekin, L.R.P. Kassab, S.A.M. Issa, C.D.S. Bordon, M.S. Al-Buriahi, F.O.P. Delboni, G. Kilic, E.S. Magalhaes, Opt. Mater. **110**, 110533 (2020).
[13] H. Kumari, K. Patel, S.K. Dhiman, S.K. Mahajan, G.F. Ansari, Mater. Today: Proc. **59**, 1127 (2022).
[14] J.L. Clabel H., J.V.P. Valverde, G. Lozano C., E. Marega Jr., V.R. Mastelaro, C.R. Mendonça, Ceram. Int. **51**, 844 (2025).
[15] O.N. Koroleva, M.V. Shtenberg, R.T. Zainullina, S.M. Lebedeva, L.A. Nevolina, Phys. Chem. Chem. Phys. **21**, 12676 (2019).